Diffraction of an extremely short optical pulse

James M. Anderson and Chandrasekhar Roychoudhuri

Photonics Research Center and Department of Electrical and Systems Engineering, University of Connecticut, Storrs, Connecticut 06269, and Anderson Photonics Plus, P.O. Box 1136, New Milford, Connecticut 06776

Received March 6, 1997; revised manuscript received September 9, 1997; accepted September 18, 1997

We provide a rigorous, closed-form mathematical model of pulsed diffraction in both time and frequency domains and interpret its anomalies. The customary continuous-wave (cw) approximation is corrected for the regime below 3 fs in pulse width, the present state of the art. The time-differentiated aspect of diffraction is linked with old theory and the conservation of energy. Convolution of the pulse with differentiated aperture edges produces traveling waves in the focal plane. Their collision near the focal point corresponds to the cw case. (This is generalized for a Gaussian beam.) Spectral sampling depicts a mode-locked laser of extremely broad spectrum, validating the nonintuitive phenomena. The square-modulus tool is validated for these pulses. Ultrashort pulses are related to data transmission rates above 100 THz. Diffraction anomalies cause confusion and loss of information in the sidelobes. Anomalous diffraction may provide new diagnostics. Diffracted energy (salient sidelobes versus continuum) can measure transform-limited pulse width. © 1998 Optical Society of America [S0740-3232(98)01202-2]

OCIS code: 050.1940.

1. INTRODUCTION

This work is concerned primarily with the precise theoretical understanding of the diffraction of extremely short pulses. Yet this subject is on the threshold of experimental relevance, since the state of the art in ultrashort pulses is about to enter the regime of the anomalous diffraction discussed here. Both single and repeated pulses are considered.

The data rate corresponding to such short pulses may be octaves above 100 THz, and the spectrum is spread from ultraviolet to infrared. It is conceivable that multiple lasers can be mode locked to produce these pulses out of their combined spectrum.

Although practical use of such short pulses seems somewhat remote, the theory presented here is appropriately contemporary with experimental efforts toward producing the pulses. In fact, one of the anomalous-diffraction phenomena can be used to measure pulse width.

While the theory is derived squarely from the old diffraction theory of Huygens, Fresnel, and Kirchhoff, it yields several unexpected conclusions. These include transverse traveling waves, time shifts in focal-plane events, and new views of old phenomena.

Simple geometries are used in this analysis, with the paraxial approximation, in the Fraunhofer plane. (A recent paper[1] examines Fresnel diffraction of ultrashort pulses but is confined to the optical axis. The single common point is our focal point and their far-field limit.) Each case considered here is represented in cross section in Fig. 1, except that a Gaussian beam replaces the aperture with a beam waist. With a plane wave normally incident on the aperture, the focal-plane pattern is obtained by integration over the aperture, with the linear time delay, $x\hat{x}/fc + y\hat{y}/fc$ in rectangular coordinates or $r\hat{r}/fc\ \cos(\theta - \phi)$ in circular coordinates, where x, y, r, and ϕ are focal-plane coordinates and $\hat{x}$, $\hat{y}$, $\hat{r}$, and θ are aperture-plane coordinates.

A long pulse is essentially a continuous wave (cw), with a slowly varying envelope, the time derivative being essentially the derivative of the sinusoid, scaled by the envelope. The present study provides the correct model for cases in which the approximation is not valid.

It is established that diffraction causes a time differentiation of the incident wave.[2] In summary of this, the Huygens–Fresnel model (Born and Wolf[3]) is interpreted for a plane wave at a rectangular aperture as

$$A = \frac{j}{f\lambda}\int_{-a}^{a}\int_{-b}^{b}\exp\left[j\omega\left(\frac{x\hat{x}}{fc} + \frac{y\hat{y}}{fc}\right)\right]\mathrm{d}\hat{y}\,\mathrm{d}\hat{x}. \qquad (1)$$

The factor $j/\lambda = j\omega/2\pi c$ is the scaled Fourier transform of the derivative operator. Given the diffraction pattern size versus wavelength, conservation of energy requires the linear frequency factor, which is consistent with the Guoy phase shift of the Gaussian-beam theory.[4,5] Time differentiation is also found in earlier studies[6,7] and is directly related to the spatial differentiation of the aperture, which may be done instead of the incident time function, with the same result. (See also passages on the Keller edge-wave theory in Ref. 8. The Keller work[9,10] actually has a very different emphasis.) Furthermore, the composite diffracted time function is Fourier transformed into a product of the Huygens–Fresnel model and a temporal spectrum (Fourier transform of the temporal pulse envelope).

This study is done in two dimensions, real slits being rectangular apertures of finite-aspect ratios (because unidimensional slits have a theoretical problem). For a rectangular aperture of dimensions, $2a$ and $2b$, the focal-plane amplitude is represented formally as

$$A(x, y, t) = \frac{1}{2\pi fc} \int_{-a}^{a} \int_{-b}^{b} \frac{\mathrm{d}}{\mathrm{d}\left(t + \frac{x\hat{x}}{fc} + \frac{y\hat{y}}{fc}\right)} \times \left\{ \psi\left(t + \frac{x\hat{x}}{fc} + \frac{y\hat{y}}{fc}\right) \times \exp\left[j\omega_c \left(t + \frac{x\hat{x}}{fc} + \frac{y\hat{y}}{fc} \right) \right] \right\} \mathrm{d}\hat{y}\, \mathrm{d}\hat{x}. \quad (2)$$

Zero time is when the temporal center of the envelope arrives at the focal point. The subscript on ω_c denotes a carrier frequency, distinct from the Fourier variable. The sinusoid at this frequency is modulated by the pulse envelope. For ψ = constant, this model reduces to the familiar cw rectangular diffraction pattern.

2. TIME-DOMAIN MODEL: RECTANGULAR APERTURE

A. Derivation

Taking ψ to be a Gaussian pulse profile, $\exp(-t^2/\tau^2)\exp[j\omega_c(t)]$, Eq. (2) becomes

$$A(x, y, t) = \frac{1}{2\pi fc} \int_{-a}^{a} \int_{-b}^{b} \times \left(\frac{t + \frac{x\hat{x}}{fc} + \frac{y\hat{y}}{fc}}{-2\frac{}{\tau^2}} + j\omega_c \right) \times \exp \frac{-\left(t + \frac{x\hat{x}}{fc} + \frac{y\hat{y}}{fc} \right)^2}{\tau^2} \times \exp\left[j\omega_c \left(t + \frac{x\hat{x}}{fc} + \frac{y\hat{y}}{fc} \right) \right] \mathrm{d}\hat{y}\, \mathrm{d}\hat{x}. \quad (3)$$

Carrying out the integration yields

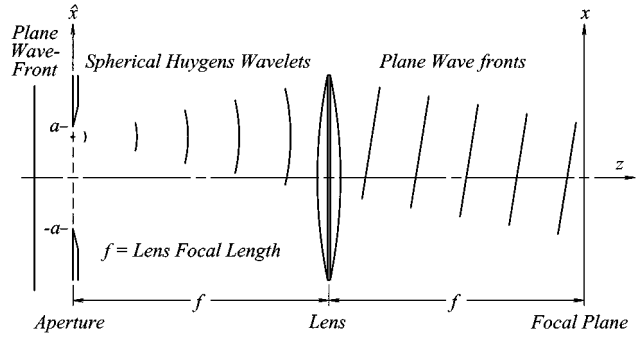

Fig. 1. Diffraction geometry of the Huygens–Fresnel model: a cross section representing a variety of aperture shapes.

$$A(x, y, t) = \frac{1}{2\pi} \frac{\sqrt{\pi}}{2} \frac{fc\tau}{xy} \exp\left(-\frac{\omega_c^2 \tau^2}{4} \right) \times \left\{ \mathrm{erf}\left(\frac{t}{\tau} + \frac{ax}{fc\tau} + \frac{by}{fc\tau} - j\frac{\omega_c \tau}{2} \right) - \mathrm{erf}\left(\frac{t}{\tau} - \frac{ax}{fc\tau} + \frac{by}{fc\tau} - j\frac{\omega_c \tau}{2} \right) - \mathrm{erf}\left(\frac{t}{\tau} + \frac{ax}{fc\tau} - \frac{by}{fc\tau} - j\frac{\omega_c \tau}{2} \right) + \mathrm{erf}\left(\frac{t}{\tau} - \frac{ax}{fc\tau} - \frac{by}{fc\tau} - j\frac{\omega_c \tau}{2} \right) \right\}. \quad (4)$$

The quartet of complex error functions (with compensating factors) replaces the product of spatial and temporal sinusoids of the cw case. Note that the multiplying factors and the argument factors may be rearranged to resemble the $(\sin \zeta)/\zeta$ factors of the cw solution. Furthermore, Eq. (4) can be Fourier transformed into the expected spectrum.

The complex-error function[11] contains all the subtle character of pulsed diffraction, with amplitude and phase modulations—consequences of focal-plane interference of time-varying wave fronts from each point in the aperture. It degenerates into the cw solution for large τ. The form of Eq. (4) is evidently four traveling waves, which collide at the focal point when $t = 0$. Each is an undifferentiated representation of the original wave incident on the aperture. The collision at the center is an indeterminate that defines differentiation.

The following transformations produce a simpler and more abstract form, designating the number of carrier cycles in τ to be n (which need not be an integer):

$$\omega_c = \frac{2\pi c}{\lambda_c}, \quad \omega_c \tau = 2\pi n, \quad \omega_c t = 2\pi\mu,$$

$$\frac{\omega_c a x}{fc} = 2\pi\xi, \quad \frac{\omega_c b y}{fc} = 2\pi\eta, \quad \frac{\omega_c a r}{fc} = 2\pi\rho,$$

$$N = 2n. \quad (5)$$

Applying Eq. (5) to Eq. (4) yields

$$A(\xi, \eta, \mu) = \frac{4ab}{f\lambda} \frac{1}{(2\pi\xi)(2\pi\eta)} \pi^{3/2} n \exp(-\pi^2 n^2) \times \left(\frac{1}{4} \right) \left\{ \mathrm{erf}\left[\frac{1}{n} (\mu + \xi + \eta - j\pi n^2) \right] - \mathrm{erf}\left[\frac{1}{n} (\mu - \xi + \eta - j\pi n^2) \right] - \mathrm{erf}\left[\frac{1}{n} (\mu + \xi - \eta - j\pi n^2) \right] + \mathrm{erf}\left[\frac{1}{n} (\mu - \xi - \eta - j\pi n^2) \right] \right\}. \quad (6)$$

B. Cross Sections

1. Spatial Cross Sections

Cross sections and snap shots are used to illustrate functions of three variables. For $\eta = 0$, L'Hospital's Rule reduces Eq. (6) to Eq. (7), a pair of traveling waves, Gaussian-modulated sinusoids of the two remaining variables:

$$A(\xi,\ \eta = 0, \mu) = \frac{4ab}{f\lambda}\frac{1}{(2\pi\xi)} \times \left(\frac{1}{2}\right)\left\{\exp\left(-\frac{1}{n^2}(\mu + \xi)^2\right) \times \exp[j2\pi(\mu + \xi)] - \exp\left(-\frac{1}{n^2}(\mu - \xi)^2\right) \times \exp[j2\pi(\mu - \xi)]\right\}. \quad (7)$$

This expression is further reduced at $\xi = 0$ to an interesting chirped-time function at the focal point:

$$\frac{4ab}{f\lambda_c}\left(-\frac{\mu}{\pi n^2} + j\right)\exp\left(-\frac{\mu^2}{n^2}\right)\exp(j2\pi\mu). \quad (8)$$

The frequency is modulated upward and back from ω_c, never less than ω_c, adding exactly one extra cycle of oscillation over the duration of the pulse.

2. Temporal Cross Sections: Snapshots

Snapshots are temporal cross sections at constant μ. The four snapshots presented in Figs. 2(a)–2(d) show the imaginary part of the amplitude for $n = 1/2$, from the temporal center of the pulse through selected later instants, showing the central standing wave (the chirped time function at the focal point) and the four receding traveling waves at three central peaks and one central zero. Notice the re-entrant spike rising out of the negative environs to reach zero in Fig. 2(c).

There are three peculiarities in the character of this pulsed combination of standing and traveling waves: (1) The central standing wave is sharply curtailed outside the temporal bounds of the pulse. (2) The traveling waves are not reduced by the pulse profile, even well outside the temporal bounds of the pulse. (3) The velocity of

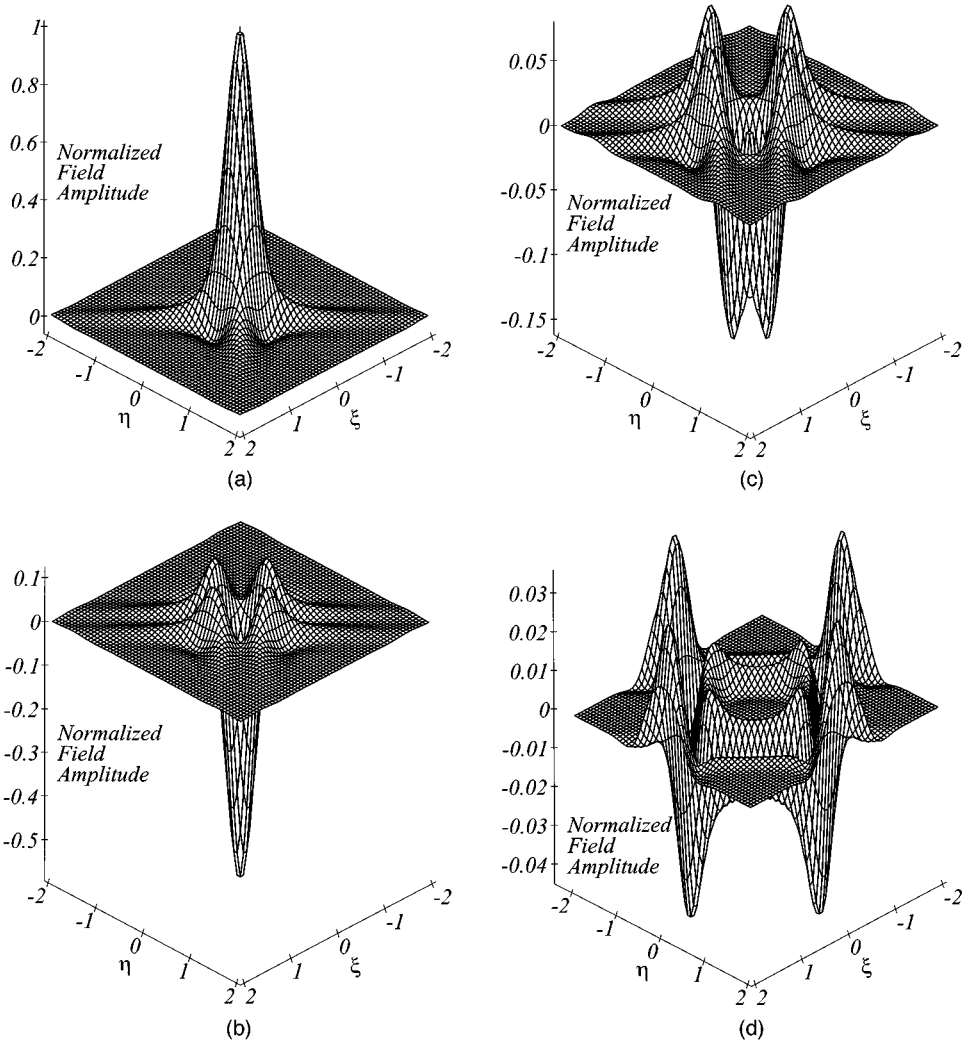

Fig. 2. Amplitude diffraction pattern of a one-cycle pulse (imaginary part). Instants of (a) peak at temporal center, (b) next peak, (c) second zero, and (d) fourth peak after temporal centers.

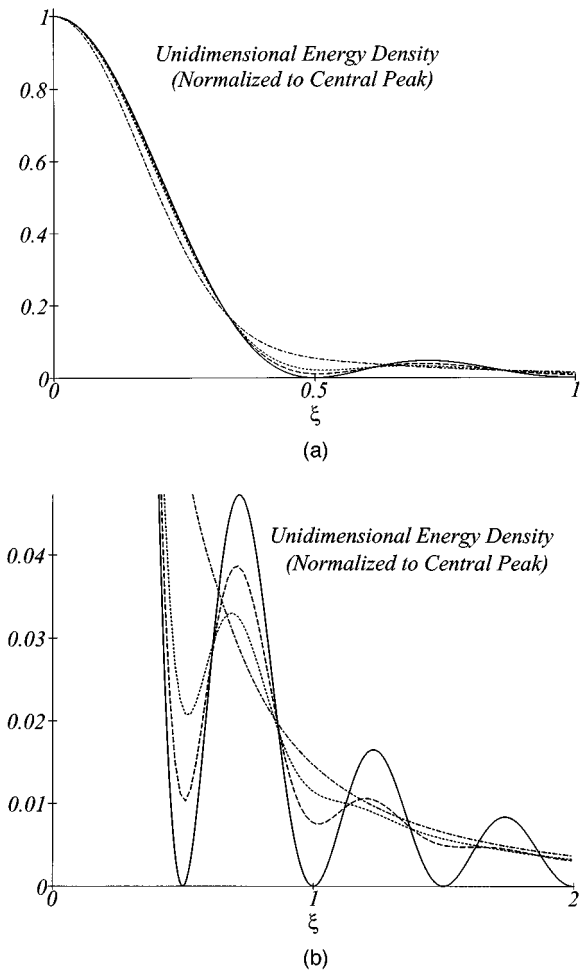

Fig. 3. Unidimensional diffracted energy density from slit for a cw (solid curve), a three-cycle pulse (dashed curve), a two-cycle pulse (dotted curve), and a one-cycle pulse (dashed-dotted curve). (a) Central pattern, (b) magnified sidelobes (b).

the traveling wave is well above the speed of light. The $1/x$ reduction in the field corresponds to the inverse square law of the intensity: a constant energy distributed over a variable area. There are two distinct velocities in the focal plane, given by $v_x = (fc)/a$ and $v_y = (fc)/b$ along the principle axes. This is similar to the transverse phase-velocity component in an optical fiber. In a relativistic view, it would be spacelike, rather than timelike.

C. Energy Density

The diffraction pattern of a narrow slit will be narrow in the opposite dimension. If the pattern is measured with a line array of photodiodes in the focal plane so as to resolve the broad dimension, the narrow dimension of the intensity will be integrated, as will the time function. This unidimensional energy density is shown in Figs. 3(a) and 3(b) for three pulse widths: three cycles, two cycles, and one cycle [full width at $\exp(-2)$ intensity].

The sidelobe pattern is a strong function of pulse width, which yields a method for determining the width of the pulses under transform-limited conditions. The number of salient sidelobes is proportional to the square of the number of cycles in the pulse, "salient" meaning a local maximum, rather than bumps on a monotone function. The three-cycle pulse has two sidelobes (or 2.25), while the two-cycle pulse has one sidelobe on each side. The single-cycle pulse has no salient sidelobes (or 0.25). Notice that the central lobe contains a decreasing portion of the total pulse energy as the pulse width is decreased.

3. FREQUENCY-DOMAIN MODEL: RECTANGULAR APERTURE

A. Basic Model

The frequency-domain model is the product of the Huygens–Fresnel model and a spectral envelope, the Fourier transform of the incident pulse time function. Given $\varphi(t) = \exp(-t^2/\tau^2)\exp(j\omega_c t)$, its spectrum is $\Phi(\omega) = (\tau/\sqrt{2})\exp\{-[(\omega - \omega_c)^2\tau^2]/4\}$, and the complete diffracted amplitude is then

$$A(x, y, \omega) = (4ab)\,\frac{j\omega}{2\pi fc}\,\frac{\tau}{\sqrt{2}}\exp\left[-\frac{(\omega-\omega_c)^2\tau^2}{4}\right] \times\left[\frac{\sin\left(\omega\,\frac{ax}{fc}\right)}{\omega\,\frac{ax}{fc}}\right]\left[\frac{\sin\left(\omega\,\frac{by}{fc}\right)}{\omega\,\frac{by}{fc}}\right]. \quad (9)$$

Each frequency component has its own scaled $\{[\sin(x)]/x\}\{[\sin(y)]/y\}$ pattern. The variable scale causes a diminution of the distinct sidelobes in the composite pattern. For each frequency component, the spatial variables are separable, whereas in the time domain all the variables are contained inseparably in the arguments of the complex error functions.

The $[\sin(\arg)]/(\arg)$ functions may be viewed as low-pass filters in ω, scaled with position in the focal plane. At the focal point, there is no filter. On either coordinate axis is a single filter. All other points experience two cascaded low-pass filters, generally of different cutoff frequencies, whose attenuation profile is ω^{-1}, with periodic zeros and phase reversals. On a diagonal, it is ω^{-2}. This character is similar for the circular aperture and rather different for the Gaussian beam.

B. Sampled Spectrum

The spectrum of Eq. (9) is a continuous function of ω, representing a single pulse. The function may be represented by a series of samples at discrete values of ω at integer multiples of a submultiple of ω_c. This produces a train of pulses, repeating at the lowest-frequency component. With a prudent choice of sampling interval and truncation of the higher frequencies, errors may be reduced to any level, the repeated pulse being identical with the original, with no significant overlap. Inverse Fourier transformation of the discrete spectrum is a simple summation instead of an integral. This yields a Fourier series, a practical compromise between an explicit analytic function and a numerical analysis.

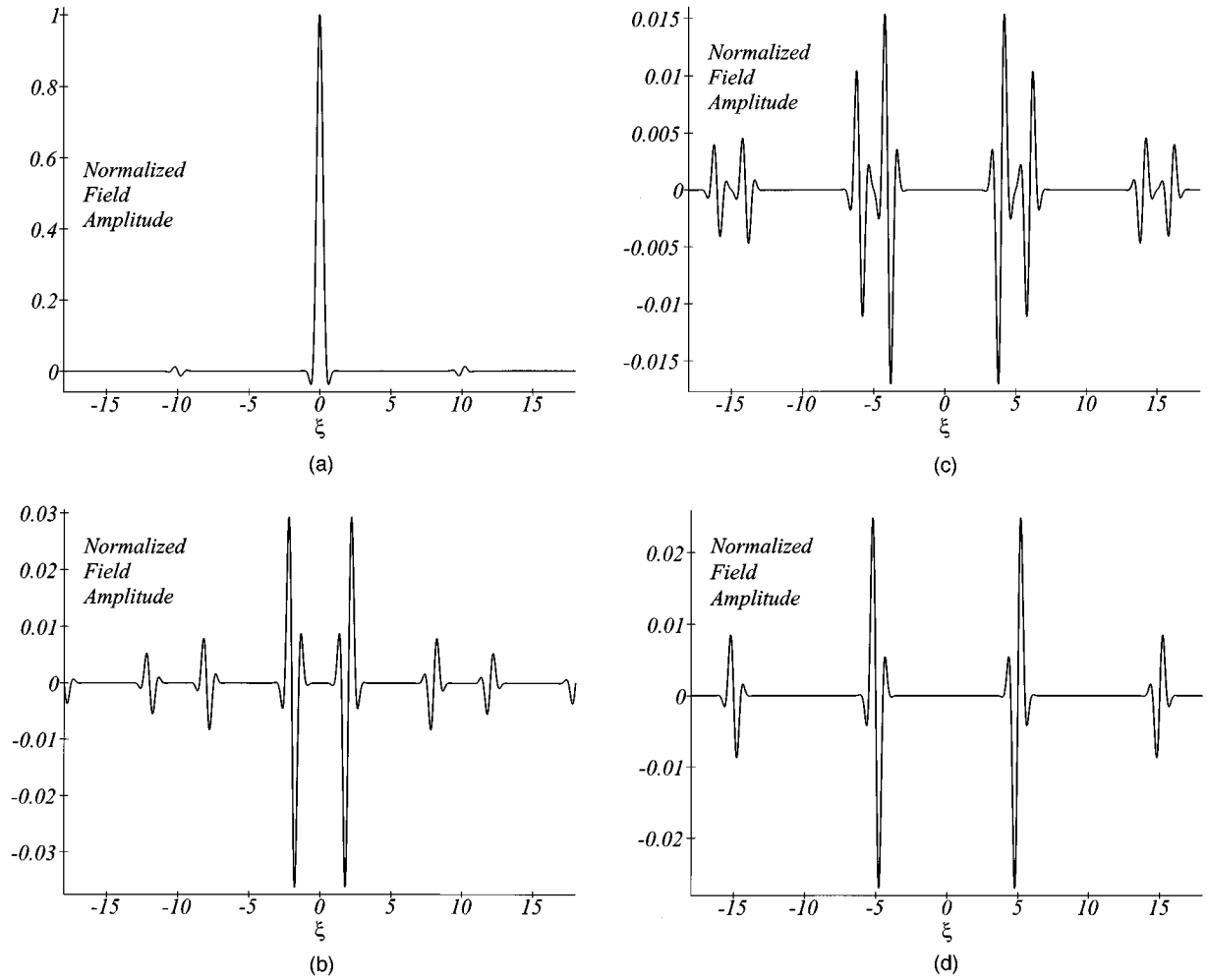

Fig. 4. Section of amplitude pattern, along the ξ axis, of a one-cycle repeated pulse (imaginary part) at (a) temporal center ($\mu = 0$), and instants later, in terms of carrier periods, by (b) $\mu = 2$, (c) $\mu = 4$, and (d) $\mu = 5$.

C. Reproducing the Time-Domain Result

Let the spectrum be sampled at discrete frequencies, $p\omega_c/P$, where p and P are integers. If we apply this in Eq. (9) with the transformations of Eq. (5), and dropping the aperture dimension factor, $(4ab)/(f\lambda)$, the normalized time function is given by

$$A_{\text{norm}}(\xi,\ \eta,\ \mu) = \sqrt{\pi}\sum_p \frac{jpn}{P^2}\exp\left[-\left(\frac{p}{P}-1\right)^2\pi^2 n^2\right] \times\left[\frac{\sin\left(2\pi\frac{p}{P}\xi\right)}{2\pi\frac{p}{P}\xi}\right] \times\left[\frac{\sin\left(2\pi\frac{p}{P}\eta\right)}{2\pi\frac{p}{P}\eta}\right]\exp\left(j2\pi\frac{p}{P}\mu\right). \tag{10}$$

For the single-cycle pulse ($n = 1/2$), for $P = 10$, and for the imaginary part, this becomes

$$A_{\text{norm}}(\xi,\ \eta,\ \mu) = \sqrt{\pi}\sum_p \frac{p}{200}\exp\left[-\left(\frac{p}{10}-1\right)^2\frac{\pi^2}{4}\right] \times\left[\frac{\sin\left(2\pi\frac{p}{10}\xi\right)}{2\pi\frac{p}{10}\xi}\right] \times\left[\frac{\sin\left(2\pi\frac{p}{10}\eta\right)}{2\pi\frac{p}{10}\eta}\right]\cos\left(2\pi\frac{p}{10}\mu\right). \tag{11}$$

With p taken from -18 to 38, this expression reproduces the snapshots presented in the time-domain analysis to less than one part in 10^9 at any point within the displayed domain, and the residual error is due to truncation of the terms and computation error rather than aliasing of the overlap of adjacent pulses. In a wider domain of

space and time, aliasing is seen in the anomalous diffraction of other pulses in the train, interacting with and overlapping the anomalous diffraction of the central pulse. The wider domain is well represented by the cross section at $\eta = 0$, in which case, Eq. (11) becomes

$$A_{\text{norm}}(\xi,\ \eta = 0,\ \mu) = \frac{1}{2}\sqrt{\pi}\sum_{p}\ \frac{p}{100}\exp\left[-\left(\frac{p}{10}-1\right)^2\frac{\pi^2}{4}\right] \times\left[\frac{\sin\left(2\pi\,\frac{p}{10}\,\xi\right)}{2\pi\,\frac{p}{10}\,\xi}\right]\cos\left(2\pi\,\frac{p}{10}\,\mu\right). \tag{12}$$

In Fig. 4(a), at $\mu = 0$, the main feature occurs at $\xi = 0$, and there are also events at $\xi = \pm 10$. These are due to the preceding and succeeding pulses, reduced by the spatial variable in the denominator. These are sine functions, whereas the central event has a cosine phase, consistent with the time differentiation near the focal point but not where the four traveling waves are separated. Furthermore, the denominator of the low-pass-filter function also acts like a time integral, which reverses the effect of the time differentiation. (Note also that at $\xi = \pm 10$ there is a resonance that brings the Fourier series components into phase for constructive interference, whereas they would otherwise destroy one another. This character is similar for the hard circular aperture but not for the Gaussian beam.)

The succeeding plots, Figs. 4(b)–4(d), show the splitting of all the events, the central event located at $\xi = 0$ and those located at $\xi = \pm 10$, each being combinations of the preceding and succeeding pulses. In Fig. 4(d), for $\mu = 5$, the central event has moved outward to $\xi = \pm 5$, while the succeeding pulse has moved inward to coincide with the (former) central event. The coincidence doubles the amplitude.

4. FREQUENCY DOMAIN: CIRCULAR GEOMETRY

A. Hard Circular Aperture

Following the format of the rectangular aperture, the Fourier series for the hard circular aperture is given by

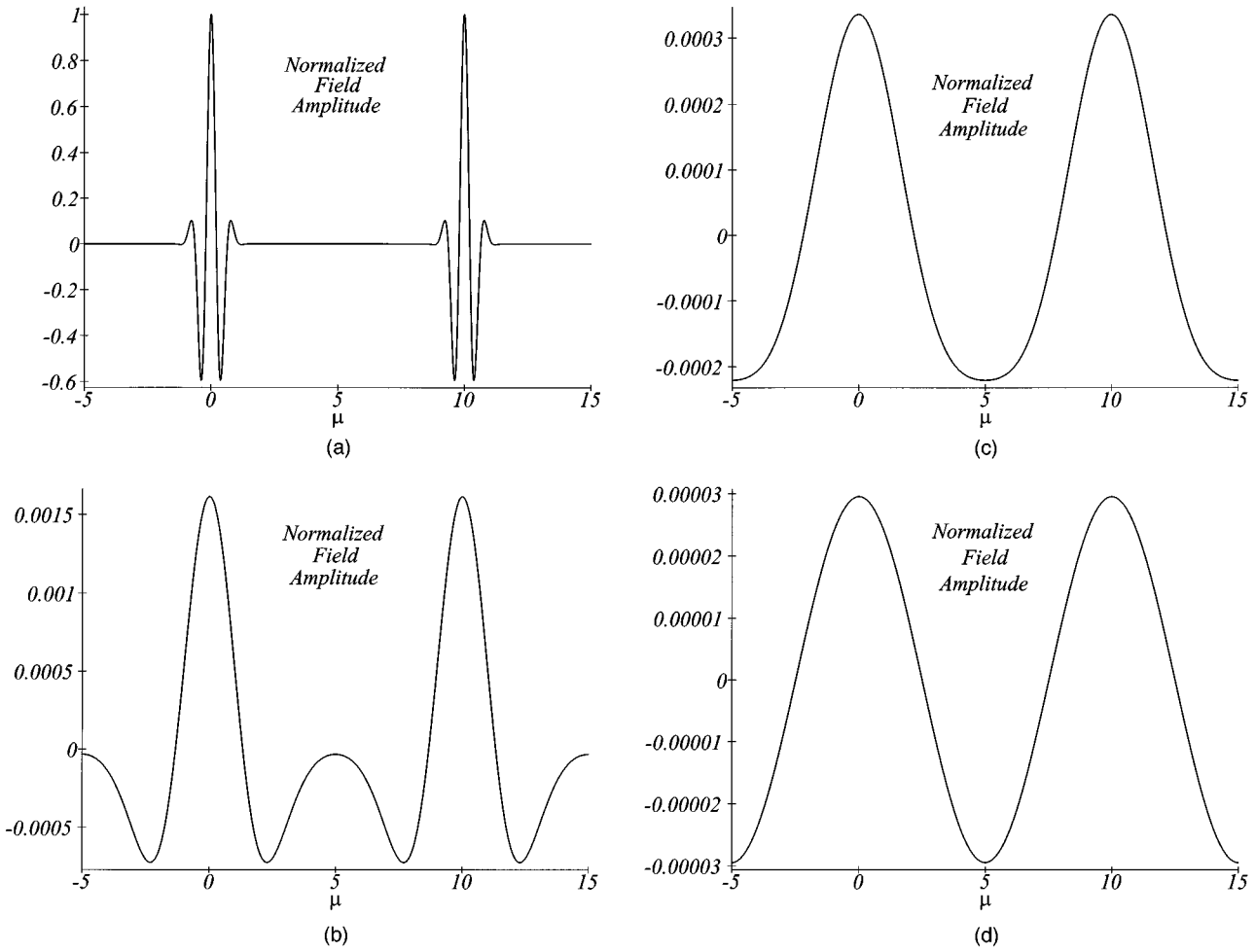

Fig. 5. Amplitude time function for a single-cycle pulsed Gaussian beam. Sampled spectrum at (a) $\rho = 0$, (b) $\rho = 3$, (c) $\rho = 5$, (d) $\rho = 9$.

$$A_{\text{norm}}(\rho,\ \mu) = \sqrt{\pi}\sum_{p} \frac{p}{200}\exp\left[-\left(\frac{p}{10}-1\right)^2\frac{\pi^2}{4}\right] \times\left[\frac{2J_1\left(2\pi\frac{p}{10}\rho\right)}{2\pi\frac{p}{10}\rho}\right]\cos\left(2\pi\frac{p}{10}\mu\right) \quad (13)$$

Here the low-pass filter is a single term with a profile of $\omega^{-3/2}$, the geometric mean between that of the principle axes and the diagonals in rectangular geometry, the extra factor of $\omega^{-1/2}$ coming from the envelope of the Bessel-function amplitude. This is similar to the rectangular case and different from the Gaussian beam.

B. Gaussian Beam

When a Gaussian beam is substituted for the uniformly illuminated hard circular aperture, each temporal-frequency component has a waist in the aperture plane of identical size. This results in a beam waist in the focal plane for each component, each with a different size, proportional to wavelength.

In addition to the procedure of the hard-aperture cases, it is necessary to find an equivalence between the size of the Gaussian beam and the circular aperture. This is done with the criteria that a circle in the focal plane contain 80% of both the Gaussian-beam energy and the Airy-disk energy and that the total energies be equal. The Gaussian-beam-waist radius in the aperture plane is equal to $2a/\pi$, where a is the radius of the hard aperture. The following expressions fulfill these criteria.

The low-pass filter for the Gaussian beam is a Gaussian function, $\exp\{-[(\omega ar)/(\pi fc)]^2\}$. This function has a much more severe attenuation profile than does the Airy disk. It affects both the temporal low-pass filter (the ω aspect of the argument) and the spatial beam geometry (the r aspect of the argument).

Since the focal-plane pattern in the time domain can be described as a convolution of the incident function with the (differentiated) aperture edges, the soft edges of the Gaussian beam spread out the convolved function—more for large radius, unlike the pair of Dirac delta functions from a hard aperture. This is responsible for strong attenuation of the oscillatory function.

With normalization, the Fourier series becomes

$$A_{\text{norm}}(\rho,\ \mu) = \sqrt{\pi}\sum_{p} \frac{p}{200}\exp\left[-\left(\frac{p}{10}-1\right)^2\frac{\pi^2}{4}\right] \times\exp\left[-\left(2\frac{p}{10}\rho\right)^2\right]\cos\left(2\pi\frac{p}{10}\mu\right). \quad (14)$$

Although this function still manifests the spatial splitting of the pulse as a function of time, the strong attenuation of the Gaussian filter affects the shape of the doughnut of energy propagated across the focal plane as it converges toward the focal point and recedes again. As a function of time, an actual splitting is not seen at all, but the pulse is temporally widened at spatial locations off center.

Spatial plots are omitted, as they contain no significant qualitative differences from the hard apertures. The time functions in Figs. 5(a)–5(d) illustrate the strong low-pass filter function of the Gaussian beam, as ρ increases from 0 to 9. In Fig. 5(a) ($\rho = 0$), with no low-pass-filter attenuation, the incident time function is modified only with a leading quadrature phase shift. In Fig. 5(b) there is a large attenuation of the higher frequencies. The pulse shape remains, although broadened, and the most dominant frequency is not the original carrier frequency but a much lower one among the Fourier components. In Fig. 5(c) the dominant frequency is the lowest Fourier component. There is no pulse character but only a slightly distorted sinusoid at the pulse repetition frequency. In Fig. 5(d) the harmonic content (distortion) is no longer perceptible, leaving essentially a pure sinusoid-monochromatic radiation at the lowest Fourier component frequency, one tenth the original carrier frequency.

C. Further Comment on Apertures

The difference between the Airy disk and the Gaussian beam is confined to the low-pass-filter factor, dominant in the outlying area of the pattern. Also of interest are intermediate cases involving softening or serrating of aperture edges in the Airy disk, as reported by Gu and Gan.[12] A thorough analysis would require many cases of transmission functions in amplitude or intensity, and the labor would be comparable with that of the cognate study of apodizing functions.

5. SUMMARY AND CONCLUSIONS

A. Mathematical Models

The frequency-domain analysis is almost always easier to do than the time-domain analysis. Represented by a discrete spectrum of frequencies, it may be conceived as the longitudinal cavity-mode spectrum of a laser. This provides credibility to the analysis. The resulting mathematical model applies to a very broad class of cases, in contrast to the severely limited class amenable to closed-form time-domain analysis. Yet it is the time-domain analysis that uncovered the pulse-splitting phenomenon obscured by the frequency-domain analysis.

The present study has shown that the discrete, Fourier series approximation verifies the striking anomalies that are explicit in the time-domain analysis. From this it is concluded that one can use the time-domain conclusions as a qualitative model for a broad range of cases and obtain more precise results with the frequency domain.

B. Experimental Work and Applications

The present state of the art in research on short pulses will allow experimental verification down to approximately two cycles of pulse width, whereas the more striking results require even shorter pulses. Since the short-pulse diffraction phenomena are not a function of the wavelength by itself, it is conceivable that such pulses

could have their carrier frequency reduced by a heterodyne technique, without corrupting the pulse envelope. This would render a pulse that is shorter in terms of cycles in the pulse. Another possibility is the use of another portion of the spectrum, such as microwave.

The extremely broad spectrum of the pulse places a substantial burden of requirements on experimental equipment. In the visible range, the spectrum may include all of the visible spectrum and some part of both the infrared and the ultraviolet.

Although no single laser could produce such a spectrum, it is not inconceivable that, say, five separate lasers at harmonically related frequencies might be mode locked to produce a train of extremely short pulses. The repetition rate of these pulses would be in the 100 THz range. In contrast to this, the highest data rates currently under consideration for optical communication use a narrow slice of spectrum in the near infrared, approximately 3 orders of magnitude less spectrum than that considered here. Present optical-fiber materials would be completely inadequate for transmission of these extremely short pulses, although point-to-point applications may be possible.

In a data-transmission application, the main conclusion regarding diffraction phenomena is that the diffracted energy does not contain the same information as that in the central portion of the pattern. It may be severely low-pass filtered, as in the case of the Gaussian beam, or it may contain a mixture of adjacent pulses, as with the hard circular aperture.

ACKNOWLEDGMENT

The authors gratefully acknowlege partial support from the Connecticut Critical Technologies Program.

REFERENCES

1. Z. Jiang, R. Jacquemin, and W. Eberhardt, "Time dependence of Fresnel diffraction of ultrashort laser pulses by a circular aperture," Appl. Opt. **36**, 4358–4361 (1997).
2. J. M. Anderson, *Diffraction of an Optical Pulse of Extremely Short Duration*, M.S. thesis (University of Connecticut, Storrs, Conn., 1997).
3. M. Born and E. Wolf, *Principles of Optics*, 6th ed. (Pergamon, Oxford, 1980), Secs. 8.2 and 8.3, pp. 370–382.
4. A. E. Siegman, *Lasers* (University Science, Mill Valley, Calif., 1986), pp. 638–647.
5. H. A. Haus, *Waves and Fields in Optoelectronics* (Prentice-Hall, Englewood Cliffs, N.J., 1984), pp. 3, 109, 114.
6. A. Lacourt, J.-C. Viénot, and J.-P. Goedgebuer, "Reassessing basic landmarks on space–time optics," Opt. Commun. **19**, 68–71 (1976).
7. J.-C. Viénot, J.-P. Goedgebuer, and A. Lacourt, "Space and time variables in optics and holography: recent experimental aspects," Appl. Opt. **16**, 454–461 (1977).
8. A. E. Siegman, *Lasers* (University Science, Mill Valley, Calif., 1986), pp. 635, 716, 723–725 and references therein.
9. J. B. Keller, "Diffraction by an aperture," J. Appl. Phys. **28**, 426–444 (1957).
10. J. B. Keller, R. M. Lewis, and B. D. Seckler, "Diffraction by an aperture II," J. Appl. Phys. **28**, 570–579 (1957).
11. National Bureau of Standards, *Handbook of Mathematical Functions* (U.S. Government Printing Office, Washington, D.C., 1964), Chap. 7, pp. 297–300.
12. M. Gu and X. S. Gan, "Fresnel diffraction by circular and serrated apertures illuminated with an ultrashort pulsed-laser beam," J. Opt. Soc. Am. A **13**, 771–778 (1996).